Microscopic aspects of wetting using classical density-functional theory

P. Yatsyshin, M.-A. Durán-Olivencia, and S. Kalliadasis

Department of Chemical Engineering
Imperial College London, London, SW7 2AZ, United Kingdom

E-mail: p.yatsyshin@imperial.ac.uk; s.kalliadasis@imperial.ac.uk

Abstract. Wetting is a rather efficient mechanism for nucleation of a phase (typically liquid) on the interface between two other phases (typically solid and gas). In many experimentally accessible cases of wetting, the interplay between the substrate structure, and the fluid-fluid and fluid-substrate intermolecular interactions brings about an entire "zoo" of possible fluid configurations, such as liquid films with a thickness of a few nanometers, liquid nanodrops and liquid bridges. These fluid configurations are often associated with phase transitions occurring at the solid-gas interface and at lengths of just several molecular diameters away from the substrate. In this special issue article, we demonstrate how a fully microscopic classical density-functional framework can be applied to the efficient, rational and systematic exploration of the rich phase space of wetting phenomena. We consider a number of model prototype systems such as wetting on a planar wall, a chemically patterned wall and a wedge. Through density-functional computations we demonstrate that for these simply structured substrates the behaviour of the solid-gas interface is already highly complex and non-trivial.

PACS numbers: 31.15.-p, 05.20.Jj, 68.08.Bc, 68.18.Jk

Submitted to: *J. Phys.: Condens. Matter*

1. Introduction

Thanks to numerous striking technological advances that took place over the past few decades, including equipment capable of high spatiotemporal resolution, fine effects associated with wetting and interface formation have become amenable to experimental scrutiny [1–3]. This, in turn, has spurred on theoreticians to explain the highly non-trivial interfacial phenomena, associated with wetting on substrates such as sculpted surfaces, pores and capillaries, where one or more characteristic dimensions are on the order of a few nanometers [4–6]. As a consequence, a number of new and exciting surface-phase transitions have recently been predicted for liquid adsorption in capped capillary pores [7–11], wedges [12–14] and other sculpted and corrugated surfaces [4, 15, 16]. As well as being of fundamental interest to the modern statistical mechanical theory of inhomogeneous fluids, developing a fundamental understanding of the way surface inhomogeneities may qualitatively affect liquid absorption and unravelling the associated highly-nontrivial surface-phase transitions, is crucial in numerous not just for wetting but for numerous other fields, such as for chemical and bioengineering, heterogeneous nucleation and crystalisation [17–20] and the rapidly growing fields of micro- and nanofluidics, including the study of formation, stability and growth of sessile nanodroplets and nanobubbles [21–23], vapour-liquid-solid growth of nanowires [24, 25], design of lab-on-a-chip devices and superhydrophobic surfaces and the burgeoning field of biomimetics [26–29],

Consider a perfectly flat wall immersed in a fluid. At the bulk liquid-gas coexistence, a macroscopic sessile drop sitting on such a wall is characterised by the Young contact angle Θ, given by the balance of the wall-gas, wall-liquid and liquid-gas interfacial tensions, $\sigma_{\rm wg}$, $\sigma_{\rm wl}$, and $\sigma_{\rm lg}$, respectively:

$$\sigma_{\rm wg} = \sigma_{\rm wl} + \sigma_{\rm lg}\cos\Theta. \tag{1}$$

A great deal of theoretical and experimental effort has been exerted to refine the simple model expressed by equation (1). But in fact, the description of wetting based on Young's contact angle is quite limited, and fails for systems with characteristic dimensions on the nanoscale. For one, the definition given in equation (1) is restricted to bulk coexistence, and it is well-known that stable nanodrops, nanobubbles, thin films and liquid bridges can be nucleated on substrate impurities from undersaturated fluid [9, 14, 21, 23, 30]. Furthermore, equation (1) reflects a local force balance at the three-phase contact line, assuming implicitly sharp interfaces, but at the nanoscale the interfaces are effectively diffuse and the menisci shapes of small drops and films are determined by the non-local intermolecular interactions, and the fluid-substrate potential, which rapidly decays with the distance from the substrate wall. Therefore, one requires a fully microscopic, non-local approach to properly capture the physics of wetting at at the nanoscale.

In the present contribution to the special issue on "Physics of integrated microfluidics", we outline an theoretical-computational framework for wetting phenomena based on the classical density-functional theory (DFT) for fluids. We

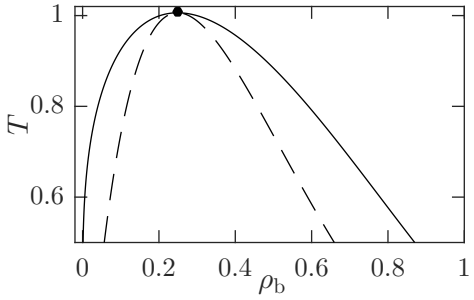


Figure 1. Bulk phase diagram of a LJ fluid in a system of units where $\varepsilon = 1$ and $\sigma = 1$ in equations (5). Full curve depicts the binodal, i.e. the locus of liquid-gas coexistence. Dashed curve depicts the spinodal, i.e. the boundary of the metastability region. The circle designates the bulk critical point at $\rho_c = 0.249$ and $T_c = 1.006$.

demonstrate the applicability and utility of the framework through model prototypical problems of wetting on patterned and sculpted planar walls. Classical DFT offers a self-consistent, computationally tractable framework, based on statistical mechanics, which can be efficiently, rationally and systematically used to scrutinise wetting phenomena at the micro- and nanoscale. Within DFT, the grand free energy of the fluid is approximated as a functional of the one-body fluid density. The free energy functional then generates a hierarchy of N-body density correlation functions, which can be used to compute observable quantities associated with wetting, such as interface contact angels, surface tensions, adsorption, etc. In particular, unconstrained minimization of the free-energy functional with respect to the one-body density yields the density profile of the inhomogeneous fluid in contact with the substrate. In this respect, classical DFT can be viewed as a means to introduce the spatial dependence of the fluid density into a thermodynamic equation of state.

In what follows, we illustrate the use of classical DFT to model wetting phenomena. We first discuss the typical ingredients of a DFT approximation and construct a minimalistic, but qualitatively reliable free-energy functional, which captures the elementary ingredients of the physics of wetting by liquid above the bulk triple point. We show how one can naturally generalise the thermodynamic method of van der Waals loops for use with a fully microscopic free-energy functional, and, for simply structured model substrates, such as patterned and sculpted planar surfaces, we compute detailed density profiles, adsorption isotherms and thermodynamic phase diagrams of wetting. Our results highlight the importance of properly taking into account very fine details of fluid–substrate intermolecular interactions for modelling wetting at the nanoscale.

2. Methodology

In this section we discuss a minimalistic fluid free-energy functional, which forms the basis for the numerical study of wetting by liquid above the bulk triple point. Detailed reviews of classical DFT can be found elsewhere [31–34].

2.1. Fluid free energy functional

Within DFT, the fluid density profiles can be obtained from an unconstrained numerical minimization of the grand free-energy functional

$$\Omega\left[\rho\left(\mathbf{r}\right)\right] = F\left[\rho(\mathbf{r})\right] - \int \mathrm{d}\mathbf{r}\ \rho\left(\mathbf{r}\right)\left(\,\mu - V\left(\mathbf{r}\right)\right), \tag{2}$$

where $F\left[\rho\left(\mathbf{r}\right)\right]$ is the intrinsic Helmholtz free-energy functional, μ is the chemical potential and $V\left(\mathbf{r}\right)$ is the cumulative external potential acting on the fluid particles from the substrate. Our approximation for $F\left[\rho\left(\mathbf{r}\right)\right]$ corresponds to the first-order Barker-Henderson [35] perturbation theory expansion of the Lennard-Jones (LJ) fluid free energy around the hard-sphere fluid free energy. Thus, our final DFT functional is equivalent to the random phase approximation for the pair-correlation function of a uniform LJ fluid. The hard sphere free-energy functional is obtained within a local density approximation, from the bulk Carnahan-Starling equation of state for the hard sphere fluid. Although the local treatment of repulsions does not allow us to recover the oscillatory behaviour of the fluid density profiles near the substrate wall, such layering effects in the fluid do not qualitatively influence the behaviour of the liquid-gas interface of the adsorbed film [36, 38].

Thus, the approximate Helmholtz free-energy functional $F\left[\rho(\mathbf{r})\right]$ of the LJ fluid in contact with a reservoir held at constant temperature T and chemical potential μ is given by the following set of equations:

$$\begin{aligned} F\left[\rho\left(\mathbf{r}\right)\right] \ &= \int \mathrm{d}\mathbf{r}\ \left[\, f_{\mathrm{id}}\left(\rho\left(\mathbf{r}\right)\right) + \rho\left(\mathbf{r}\right)\psi\left(\rho\left(\mathbf{r}\right)\right)\right] \\ &\quad + \frac{1}{2}\int \mathrm{d}\mathbf{r}\int \mathrm{d}\mathbf{r}'\ \rho\left(\mathbf{r}\right)\rho\left(\mathbf{r}'\right)\varphi_{\mathrm{attr}}\left(|\mathbf{r}-\mathbf{r}'|\right), \end{aligned} \tag{3}$$

where $f_{\mathrm{id}}\left(\rho\right) = k_{\mathrm{B}}T\rho\left(\ln\left(\lambda^3\rho\right) - 1\right)$ is the ideal gas free-energy density, and λ is the thermal wavelength; $\psi\left(\rho\right)$ is the Carnahan-Starling free-energy density of the bulk hard sphere fluid:

$$\psi\left(\rho\right) \ = \ k_{\mathrm{B}}T\ \frac{\eta\left(4-3\eta\right)}{\left(1-\eta\right)^2}, \qquad \eta = \pi\sigma^3\rho/6, \tag{4}$$

where σ is the hard sphere diameter and $\varphi_{\mathrm{attr}}\left(|\mathbf{r}-\mathbf{r}'|\right)$ is the attractive part of the potential given by the Barker-Henderson approximation:

$$\varphi_{\mathrm{attr}}\left(r\right) = \begin{cases} 0, & r \le \sigma \\ \varphi^{\mathrm{LJ}}_{\sigma,\varepsilon}(r), & r > \sigma, \end{cases} \tag{5}$$

where $\varphi^{\mathrm{LJ}}_{\sigma_0,\varepsilon_0}$ is the LJ potential:

$$\varphi^{\mathrm{LJ}}_{\sigma_0,\varepsilon_0}(r) = 4\varepsilon_0\left[\left(\frac{\sigma_0}{r}\right)^{12} - \left(\frac{\sigma_0}{r}\right)^{6}\right]. \tag{6}$$

The density profiles $\rho\left(\mathbf{r}\right)$ minimizing the grand free-energy functional $\Omega\left[\rho\left(\mathbf{r}\right)\right]$ satisfy the Euler–Lagrange equation:

$$\begin{aligned} &k_{\mathrm{B}}T\ln\rho\left(\mathbf{r}\right) + \psi\left(\rho\left(\mathbf{r}\right)\right) + \rho\left(\mathbf{r}\right)\psi'_{\rho}\left(\rho\left(\mathbf{r}\right)\right) \\ &+ \int d\mathbf{r}'\rho\left(\mathbf{r}'\right)\varphi_{\mathrm{attr}}\left(|\mathbf{r}-\mathbf{r}'|\right) + V\left(\mathbf{r}\right) - \mu = 0, \end{aligned} \tag{7}$$

where ψ'_ρ is the derivative of $\psi(\rho)$ in equation (4) with respect to ρ. As already mentioned earlier, classical DFT can be viewed as a generalization of thermodynamic equation of state to include the inhomogeneous fluid structure. This becomes apparent by considering the bulk limit of equations (2) and (7), where $\rho(\mathbf{r}) \to \rho_\mathrm{b} = \mathrm{const}$ (bulk density) and $V(\mathbf{r}) \to 0$:

$$\mu = k_\mathrm{B}T \ln \rho_\mathrm{b} + \psi(\rho_\mathrm{b}) + \rho_\mathrm{b}\psi'_{\rho_\mathrm{b}}(\rho_\mathrm{b}) - \frac{32\pi}{9}\rho_\mathrm{b}\sigma^3\varepsilon, \tag{8}$$

$$P = \rho_\mathrm{b}k_\mathrm{B}T\frac{1+\eta+\eta^2-\eta^3}{(1-\eta)^3} - \frac{16\pi}{9}\rho_\mathrm{b}^2\sigma^3\varepsilon, \tag{9}$$

where P denotes the bulk pressure, and we have made use of the thermodynamic relation

$$\Omega[\rho_\mathrm{b}] = -PV. \tag{10}$$

At bulk liquid-gas coexistence (saturation), $\mu(\rho_\mathrm{l}) = \mu(\rho_\mathrm{g}) = \mu_\mathrm{sat}$ and $P(\rho_\mathrm{l}) = P(\rho_\mathrm{g}) = P_\mathrm{sat}$ (saturation pressure). Solving these equation for a range of temperatures, we can obtain the bulk liquid-gas phase diagram (bulk binodal). At the boundaries of metastability of the super-saturated gas and liquid (bulk spinodals), we have $\partial P/\partial\rho\,|_{\rho_\mathrm{g},\rho_\mathrm{l}} = 0$. The bulk critical point at $T = T_\mathrm{c}$ and $\rho = \rho_\mathrm{c}$, satisfies the equations $\partial P/\partial\rho_\mathrm{c} = \partial^2 P/\partial\rho_\mathrm{c}^2 = 0$. The bulk binodal and spinodal, computed by solving the above equations are depicted in figure 1. In what follows, we demonstrate how the same thermodynamic analysis which allows us to compute the bulk phase diagram, can also be used to investigate inhomogeneous fluids near adsorbing surfaces. Such methodology is based on the fact that for any given T and μ of the reservoir, we can obtain $\rho(\mathbf{r})$ by solving equation (7) and the corresponding grand potential $\Omega(T,\mu)$ from equation (2). Further details on the approximations involved in (3)–(7), as well as details on the numerical scheme used to solve equation (7) in one and two spatial dimensions can be found elsewhere [14, 37, 38].

The intrinsic Helmholtz free-energy functional $F[\rho(\mathbf{r})]$ does not depend on the external potential $V(\mathbf{r})$, which enters the expression for the grand free energy in equation (2) and accounts the forces exerted on the fluid from the substrate. For a given substrate, the potential $V(\mathbf{r})$ can be obtained by integrating the LJ fluid-substrate interactions in equation (6) with the substrate-specific parameters ε_0 and σ_0 over the substrate volume.

$$V(\mathbf{r}) = \rho_0 \int \varphi^{\mathrm{LJ}}_{\sigma_0,\varepsilon_0}(|\mathbf{r}-\mathbf{r}'|)\, d\mathbf{r}', \tag{11}$$

where ρ_0 is the effective density of the substrate material. The problem with equation (11) is that the formally obtained potential $V(\mathbf{r})$ would have a non-physical divergence at fluid-substrate contact. To eliminate this divergence, we will assume that the surface of the substrate is coated with a layer of an inert material of width H_0. This is a purely mathematical device and does not affect the physics of wetting, which is determined by the long-range tail of the fluid-substrate interaction potential [36, 38].

3. Results and discussion

For the computations presented here we choose the system of units, where the hard-core diameter σ and the well depth ε of the fluid–fluid LJ interactions in equation (5) are set as units of length and energy. Since we focus on wetting by liquid, where the stable bulk thermodynamic phase is gas, it is most convenient for us to plot the isotherms and phase diagrams in the T–$\Delta\mu$ plane, where $\Delta\mu\,(T) = \mu - \mu_{\rm sat} \leq 0$ is the deviation of the chemical potential from the saturation value at $\mu_{\rm sat}$. Without loss of generality, for each substrate material considered, we set the effective substrate density $\rho_0 = 1$ in equation (11) and $\sigma_0 = 2$ in equation (6). We further set the coating parameter $H_0 = 5$ in equations (12), (17) and (21) (see below).

3.1. Homogeneous planar wall

Consider a model system with an ideally flat planar wall mentioned in the Introduction. The substrate potential $V(\mathbf{r})$ in equation (2) depends only on the distance y in the normal direction from the wall

$$V_0\,(y) = 4\pi\varepsilon_0\sigma_0^3\left[-\frac{1}{6}\left(\frac{\sigma_0}{H_0+y}\right)^3 + \frac{1}{45}\left(\frac{\sigma_0}{H_0+y}\right)^9\right], \tag{12}$$

where $\rho_{\rm w}$ is the average density of the substrate material and H_0 is the wall coating, introduced to avoid the non-physical divergence of $V_0\,(y)$ at $y = 0$, and to reduce the fluid–substrate repulsions [those are not properly captured by (3) anyway]. The effect of varying the finite fixed $H_0 > 0$ is investigated in, e.g., Appendix 1 of Reference [38], where it is shown that such low-y cut-offs do not qualitatively affect the planar wetting phenomenology.

To use the DFT computations in conjunction with the standard thermodynamic method of van der Waals loops to uncover surface-phase transitions, occurring during the wetting of the solid-gas interface by liquid, we need to define an appropriate order parameter for such transitions. In wetting problems, a convenient choice is adsorption, which, in general, can be defined as an excess amount of matter, adsorbed at the interface undergoing a transition. Since during wetting of a planar homogeneous wall the fluid density profile can change only along y, $\rho(\mathbf{r}) \equiv \rho(y)$, we can define the adsorption Γ_0 relatively to the bulk fluid density $\rho_{\rm b}$:

$$\Gamma_0 = \int\limits_0^\infty dy\;[\,\rho\,(y) - \rho_{\rm b}\,]\,. \tag{13}$$

The thermodynamic conjugate to adsorption is the excess grand potential $\Omega_{\rm ex}$, which is related to it through the Gibbs equation:

$$\Gamma_0\,(\mu) = -\frac{1}{A}\left(\frac{\partial\Omega_{\rm ex}}{\partial\mu}\right)_T, \tag{14}$$

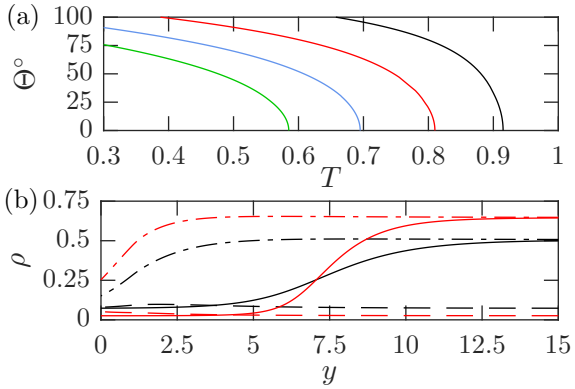


Figure 2. (a) Young contact angles of planar homogeneous walls with $\varepsilon_{\rm w} = 1$, 0.8, 0.6 and 0.4 (left to right). (b) Density profiles for $\Theta = 50°$, and $\varepsilon_{\rm w} = 0.6$ ($T = 0.745$, red) and $\varepsilon_{\rm w} = 0.4$ ($T = 0.880$, black). Solid curves correspond to the coexisting bulk liquid and gas, and dashed and dashed-dotted curves correspond to the saturated liquid and gas in contact with the wall.

where A is the wall area. It is straightforward to see that, given a density profile, $\Omega_0^{\rm ex}$ can be computed from the following equation:

$$\Omega_0^{\rm ex} = \Omega\left[\rho\left(y\right)\right] - \Omega\left[\rho_{\rm b}\right]. \tag{15}$$

During a phase transition, the grand free energies of the coexisting fluid phases must be equal. It follows from equations (13) and (15) that interface phase coexistence is associated with a hysteresis of the adsorption isotherm $\Gamma_0\left(\mu\right)$, and that the coexisting fluid configurations correspond to an equal area construction, performed on the hysteresis S-loop of the adsorption isotherm $\Gamma_0\left(\mu\right)$. The regions of metastability (spinodals) are, in turn, demarcated by the loci of the turning points of adsorption isotherms.

First, let us use the DFT free-energy functional to compute the Young contact angle of a macroscopic sessile drop from equation (1). Surface tension is the interface energy per unit area. Therefore, according to equations (10) and (15), given the density profile $\rho\left(y\right)$ of a saturated fluid, each interfacial tension σ in equation (1) can be computed from the following equation

$$\sigma = \frac{1}{\mathcal{L}}\Omega\left[\rho\left(y\right)\right] + PV. \tag{16}$$

Thus, after obtaining the density profiles of the saturated liquid and gas in contact with the wall (by solving equation (7) with $V(\mathbf{r})$ given in equation (12)), and the coexisting liquid and gas density profile (by solving equation (7) with $V(\mathbf{r}) \equiv 0$), we can compute the surface tensions and the corresponding Young contact angles. Several representative examples of $\Theta(T)$ of different wall-fluid potentials are represented in figure 2(a). It is noteworthy that the Young angle vanishes at what is called the substrate wetting temperature, $T_{\rm w}$. As a matter of fact, for $T \to T_{\rm w}$ the Young angle follows a power law $\Theta(T) = \mathcal{O}(T_{\rm w} - T)^{1/2}$, where the exponent $1/2$ is universal, i.e. it does not depend on the nature of the intermolecular forces [39]. As is also evident from figure 2 that stronger

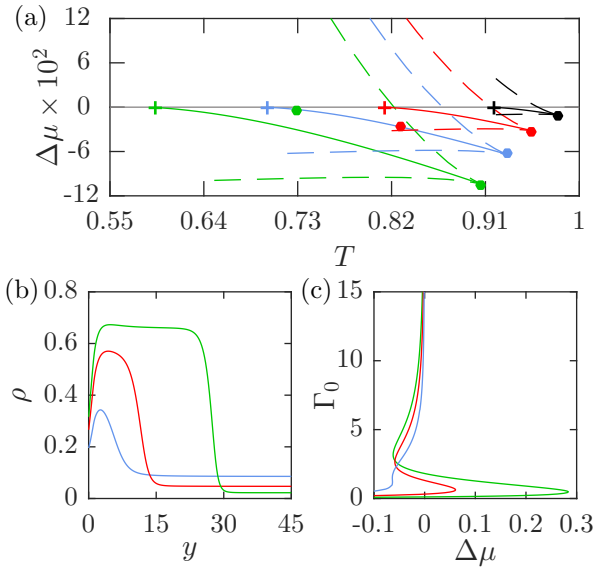


Figure 3. (a) Planar pre-wetting lines of walls from figure 2 (solid curves) and respective spinodals (dashed curves). The wetting temperatures are $T_{\rm w} = 0.59$, 0.70, 0.81 and 0.92 (left to right, designated by "+" signs). The respective critical pre-wetting temperatures are $T_{\rm pw}^{\rm c} = 0.91$, 0.93, 0.95 and 0.98 (designated by filled circles). (b) Representative density profiles of the coexisting thick films at $T = 0.73$, 0.83 and $0.93 (= T_{\rm pw}^{\rm c})$, along the pre-wetting line of the wall with $\varepsilon_{\rm w} = 0.8$ [also marked by filled coloured circles in (a)]. (c) Corresponding adsorption isotherms.

substrates (with higher ε_0) have lower wetting temperatures. On the macroscopic level, at saturation and $T = T_{\rm w}$, the wall becomes fully covered by a liquid film, instead of isolated sessile drops with finite contact angles. This phenomenon is known as the *wetting transition* and can be first-order or continuous, depending on the nature of the intermolecular forces [2, 39, 40].

In figure 2(b) we plot several representative density profiles of the saturated fluid at two different temperatures, but the same Young angle $\Theta = 50°$. We see that a lower temperature corresponds to sharper interfaces, which is particularly prominent in the case of a free liquid-gas interface. Similarly, lower Ts are associated with bigger coexisting liquid densities, but smaller coexisting gas densities, as is also evident from the bulk phase diagram in figure 1. The density functional in equation (3) is mean-field, and thus does not capture the effects of capillary waves, which may broaden the liquid-gas interfaces in weak external fields, or the bulk critical fluctuations, whose correlation length diverges in the limit $T \to T_{\rm c}$ [41]. It is also noteworthy that since the hard sphere part of our free-energy functional is local in density, the computed density profiles do not exhibit any near-wall layering, which typically is present in the fluid [37]. More sophisticated non-local hard sphere functionals should be used in equation (3) to investigate fluid layering and freezing [33]. Nevertheless, our DFT provides a satisfactory qualitative description of the liquid-gas interface at temperatures between the bulk triple point and the bulk critical temperature [33, 42].

A rather interesting and important feature of wall wetting is a bi-stability occurring in thin adsorbed liquid films, known as the *pre-wetting transition* [15, 43]. On homogeneous walls, pre-wetting is a first-order transition associated with a jump from a thin to a thick layer of liquid adsorbed on the wall, as $\Delta\mu$ is increased towards saturation. The adsorption defined in equation (13) undergoes a jump at pre-wetting. First-order wetting walls usually have a line of the thin-thick film transitions, $\Delta\mu_{\rm pw}(T)$, which approaches saturation tangentially at $T_{\rm w}$. By computing the transition from the S-shaped loops of adsorption isotherms at different temperatures, we construct the phase diagrams of pre-wetting transitions for our selection of $\varepsilon_{\rm w}$ of the wall-fluid LJ potential, depicted in figure 3(a). We also compute the spinodals of the pre-wetting line, which demarcate the boundaries of metastability of the thick adsorbed films. These spinodals are associated with the turning points of the isotherms $\Gamma_0(\mu)$. For LJ forces, the vanishing of the pre-wetting line near bulk saturation follows a non-universal power law $\Delta\mu_{\rm pw}(T) = \mathcal{O}(T - T_{\rm w})^{3/2}$ [11, 14].

Figure 3(b) shows a set of representative density profiles of thick coexisting films along one of the pre-wetting lines [marked by circles in figure 3(a)]. The profiles have near-constant plateaus of density, which correspond to bulk coexisting liquid and gas, and unbind as saturation is approached. As already mentioned, according to equation (13) and (14), pre-wetting transitions correspond to an equal area construction on the hysteresis loop of the adsorption isotherms $\Gamma_0(\mu)$ at $\mu = \mu_{\rm pw}$. Several representative plots of $\Gamma_0(\mu)$, including the critical one with respect to pre-wetting, are given in figure 3(c). We note the divergence of $\Gamma_0(\mu)$ at $\mu \to \mu_{\rm sat}$. As a matter of fact, the adsorbed film thickness diverges with a non-universal power-law $h = \mathcal{O}(\Delta\mu^{-1/3})$, which is determined by the long-ranged decay of the LJ forces [44].

3.2. Striped wall

Consider introducing a defect into the planar wall prototype of the previous section, in the form of a deep narrow stripe of width L. The potential exerted on the fluid by such inhomogeneous wall can be obtained by integrating the pairwise LJ fluid–substrate potentials of the individual materials of the wall, $\varphi^{\rm LJ}_{\sigma_{\rm w},\varepsilon_{\rm w}}(r)$, and the stripe, $\varphi^{\rm LJ}_{\sigma_{\rm s},\varepsilon_{\rm s}}(r)$, over the volumes occupied by each:

$$V_L(x,y) = V_0(y) - \int\limits_{\nu_L} \varphi^{\rm LJ}_{\sigma_{\rm w},\varepsilon_{\rm w}}(|\mathbf{r}-\mathbf{r}'|)\,{\rm d}\mathbf{r}' + \int\limits_{\nu_L} \varphi^{\rm LJ}_{\sigma_{\rm s},\varepsilon_{\rm s}}(|\mathbf{r}-\mathbf{r}'|)\,{\rm d}\mathbf{r}', \qquad (17)$$

where the integration is carried out over the volume ν_L of the stripe of width L, excluding the coating: $\nu_L = \{(x,y,z) : -L/2 \le x \le L/2, -\infty < y \le -H_0, -\infty < z < \infty\}$. On the striped wall, the fluid density can change in two directions, $\rho(\mathbf{r}) \equiv \rho(x,y)$, and it is convenient to define excess adsorption per unit length along the wall (order parameter for transitions), Γ_L, relatively to adsorption on a uniform wall:

$$\Gamma_L = \int\limits_{-\infty}^{\infty} dx \int\limits_{0}^{\infty} dy\ \left[\,\rho_L(x,y) - \rho_{L=0}(y)\right], \qquad (18)$$

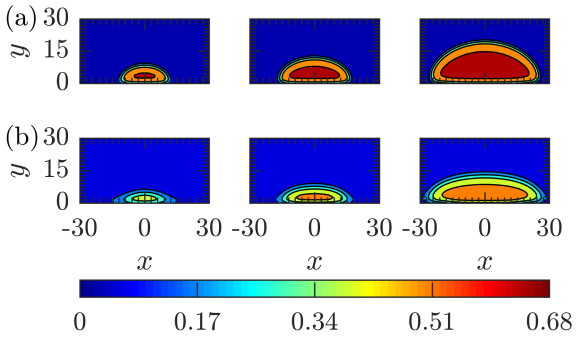


Figure 4. Fluid at a planar wall with $\varepsilon_{\rm w} = 0.6$ and $T_{\rm w}^{\rm (w)} = 0.81$, decorated with a stronger adsorbing stripe with $\varepsilon_{\rm s} = 1$ and $T_{\rm w}^{(s)} = 0.60$ of width $L = 32$, positioned at $16 \leq x \leq 16$. (a) Fluid density profiles at $T = 0.74(< T_{\rm w}^{\rm (w)})$ and wall Young angle $\Theta_{\rm w} = 52.3°$, at $\Delta\mu = (-12.09, -0.17, 11.67) \times 10^{-3})$ (left to right). The last profile is metastable. (b) Fluid density profiles at $T = 0.88(> T_{\rm w}^{\rm (w)})$, at $\Delta\mu = (-7.3, -5.6, -1.9) \times 10^{-2}$, which approaches planar pre-wetting at $\Delta\mu_{\rm pw}^{\rm (w)} = -1.1 \times 10^{-2}$.

where $\rho_L(x, y)$ and $\rho_{L=0}(y)$ are the fluid density profiles on the striped wall and in the absence of the stripe, respectively, computed at the same values of T and μ. The conjugate excess grand potential of a striped wall, $\Omega_L^{\rm ex}$ is given by

$$\Omega_L^{\rm ex} = \Omega\left[\rho_L(x, y)\right] - \Omega\left[\rho^{\rm (w)}(x)\right]. \tag{19}$$

A number of recent works were dedicated to adsorption on chemically nanopatterned planar walls [45–49]. Developing a deeper appreciation of the mechanisms effecting the local height of the liquid-gas interface near nanoscopic chemical inhomogeneities is crucial for our understanding of the changes between the so-called Wenzel and Cassie–Baxter states of sessile drops. Very importantly, nanoscale chemical patterns can dramatically change the phenomenology of wetting. Consider a wall, decorated with a stripe of a stronger adsorbing material. The fluid-wall potential is given by equation (17). The stronger material of the stripe can stabilize liquid at the surface of the stripe, adsorbed from undersaturated gas. In figure 4 we represent density profiles of undersaturated fluid in contact with a striped wall, at temperatures above [figure 4(a)] and below [figure 4(b)] the wetting temperature $T_{\rm w}^{\rm (w)}$ of the homogeneous outer wall. Evidently, below the wall wetting temperature, there is a local condensation of liquid on the stripe, which is driven by the competition between the attractive fluid-substrate interactions and the surface tension forces at the liquid-gas interface. The nanodrops formed below saturation are thermodynamicaly stable, due to their pinning by the stripe. They grow in size as $\Delta\mu \to 0$, and may remain metastable even above bulk saturation.

Above $T_{\rm w}^{\rm (w)}$, the stripe nucleates a thick pre-wetting film, which spreads out along the wall as $\mu \to \mu_{\rm pw}^{\rm (w)}$ [16,49]. This finding is particularly important, because, as we have seen, the pre-wetting transition from thin to thick film is discontinuous on homogeneous walls. Thus, the nanostripe not only stabilizes nanoscale fluid configurations, but alters the physics of the larger-scale phenomenon of pre-wetting. It can be shown that for

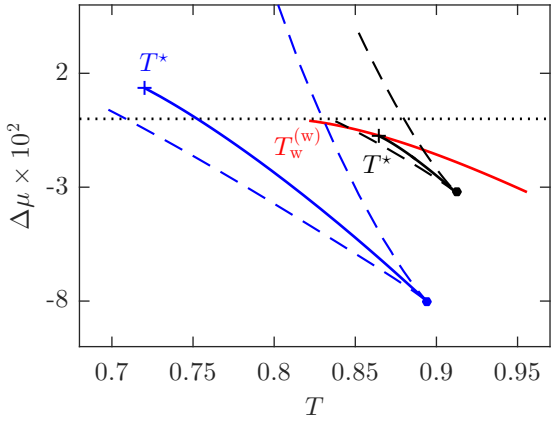


Figure 5. Phase diagram of wetting on striped walls with stripe widths $L = 32$ (solid blue) and $L = 8$ (solid black). The fluid-substrate LJ parameters are the same as in figure 4. The respective low-T boundaries of the unbending lines (designated by "+"-signs) are at $T^* = 0.72$ and $T^* = 0.87$. Critical unbending points are designated by filled circles. The red curve corresponds to the pre-wetting line of the homogeneous (w)-wall. The spinodals of unbending (dashed curves) demarcate the regions of metastability of the fluid configurations shown in figure 4.

LJ fluid-substrate intermolecular forces, the lateral dimension of the adsorbed thin film grows as $\mathcal{O}(\mu_{\rm pw}^{(w)} - \mu)^{-1/4}$, as $\mu \to \mu_{\rm pw}^{(w)}$ with a non-universal critical exponent [16].

The formation of the nanodrops in figure 4(a) is discontinuous within a mean-field framework, and is associated with a jump in adsorption given in equation (18). This first-order transition is known as the *unbending transition*, and was originally found as a flattening of the liquid-gas interface during adsorption on walls, decorated with nanotroughs [46, 49]. In order to put interface unbending in context with wetting of a homogeneous wall, it is instructive to consider complete wetting phase diagrams, represented in figure 5 for a patterned wall with stripes of widths $L = 8$ and $L = 32$. The unbending transition lines $\mu_{\rm u}(T)$ and their respective spinodals were computed by tracing the hysteresis loops and turning points of adsorption isotherms for $\Gamma(\mu)$ defined in equation (18), computed for different temperatures. We see that the unbending line of a wider stripe crosses the saturation line and terminates in the region of stable bulk liquid, at $T = T^* \approx 0.72$. Of-course, at $\Delta\mu > 0$, the nanodrop formation is pre-empted by saturation. Therefore, the part of the transition line at $\Delta\mu > 0$ is spurious, and is simply the result of equation (7) having drop-like solutions at $\Delta\mu > 0$. Nevertheless, the boundaries of metastability of nanodrops are given by the spinodals of $\Gamma(\mu)$. The fact that the spinodals extend deep into the supersaturated liquid (the region $\Delta\mu > 0$), means that in principle there is a possibility of the existence of sizable metastable nanodrops. This is also confirmed by recent studies [21, 30].

Even more interesting features are revealed by the unbending line of the narrower stripe with $L = 8$. First of all, since the entire transition line and its spinodals lie above the substrate wetting temperature, this stripe can only nucleate (meta)stable films. Secondly, that the unbending line approaches pre-wetting tangentially signifies

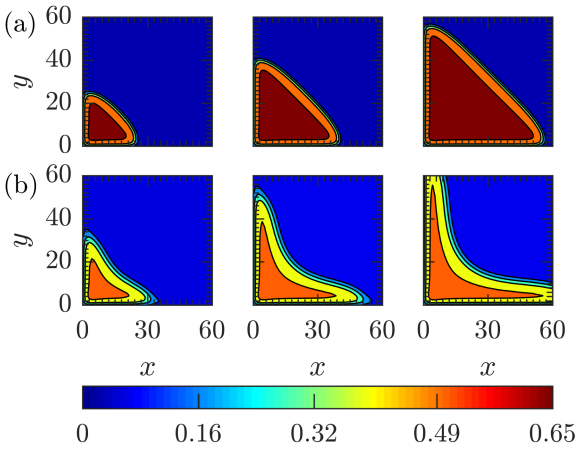


Figure 6. Liquid adsorption in a right-angle wedge with the depth of the wall-fluid potential well $\varepsilon_{\rm w} = 0.6$. The planar wetting temperature $T_{\rm w} = 0.755$. The wedge filling temperature $T_{\rm f} = 0.693$. (a) Density configurations at $T = 0.73 (< T_{\rm w})$, $\Theta = 28.33^\circ$ and μ approaching bulk coexistence: $\Delta\mu = (-0.50, -0.40, -0.33)\times 10^{-2}$(left to right). (b) Density configurations at $T = 0.88$ $(> T_{\rm w})$, below the pre-wetting transition (at $\Delta\mu_{\rm pw} = -0.25 \times 10^{-1}$), at μ approaching pre-wetting: $\Delta\mu = (-0.33, -0.28, -0.26) \times 10^{-1}$ (left to right).

the already mentioned finding that pre-wetting transition changes order, due to chemical patterning of the wall. Everywhere above T^*, the pre-wetting transition is continuous. Using the surface Clausius-Clapeyron equation, it is easy to work out the asymptote of the vanishing distance between the unbending and prewetting lines of narrow stripes, near T^*: $\mu_{\rm pw}(T) - \mu_{\rm u} = \mathcal{O}(T - T^*)^{4/3}$ [49].

3.3. Wedge

We can gain insight about wetting on geometrically corrugated substrates by studying liquid adsorption in a prototypical model consisting of a wedge-shaped pore in ambient undersaturated gas. Therefore, consider two planar walls, meeting at an opening angle α. As was first pointed out by Hauge [50], liquid condensed in the wedge apex must necessarily have a concave meniscus with the surrounding vapour. This provides a restriction on the Young angles of the liquid meniscus with the wedge walls:

$$\Theta(T) \leq \pi/2 - \alpha/2. \tag{20}$$

The equality in the above expression corresponds to a flat liquid-gas interface and defines the wedge filling temperature, $T_{\rm f} < T_{\rm w}$, where the *wedge filling transition* occurs [12,51]. For a given wedge, this temperature can be computed with DFT from the dependence $\Theta(T)$, such as the ones shown in figure 2.

In the present work we are more interested in small amounts of liquid adsorbed at the wedge apex. Therefore, we apply our DFT framework to the case $\alpha = \pi/2$. The fluid-substrate potential $V(\mathbf{r})$ in equation (2) acting on the fluid is then given by

$$V_{\rm wdg}(x, y) = V_0(x) + V_{\rm q}(-x - H_0, y), \tag{21}$$

where $V_{\mathrm{q}}(x,y)$ is the potential of a square quadrant ($x \leq 0, y \leq 0, -\infty < z < \infty$):

$$V_{\mathrm{q}}(x,y) = \int_{-\infty}^{\infty} \mathrm{d}z' \int_{-\infty}^{0} \mathrm{d}y' \int_{-\infty}^{0} \mathrm{d}x' \varphi^{\mathrm{LJ}}_{\epsilon_0,\sigma_0}\left(\sqrt{(x-x')^2+(y-y')^2+z'^2}\right). \tag{22}$$

Figure 6 depicts several representative fluid density profiles, corresponding to wedge wetting below [figure 6(a)] and above [figure 6(b)] the planar wetting temperature, and different values of undersaturation. We can see that at $T_{\mathrm{f}} < T < T_{\mathrm{w}}$, the filling of the wedge proceeds continuously, via an unbinding flat meniscus. Empirically, the flat shape of the meniscus is to be expected, because curvature increases the free energy of the fluid interface. However, as saturation is approached, the amount of adsorbate grows and the influence of one wall on the contact angle with the other wall becomes negligible. Therefore, near saturation the liquid meniscus will rich the macroscopic values of the contact angle, given by the Young angle. Above T_{w}, we again observe continuous pre-wetting transition, where the thick pre-wetting film, nucleated at the wedge apex unbinds along the walls of the wedge. The growth of the liquid film along the wall as a function of μ is proportional to $(\mu_{\mathrm{pw}} - \mu)^{-1/4}$, where the non-universal exponent is linked to the potential of the LJ intermolecular forces.

Additionally, the mean-field DFT framework would pick up a transition, similar to pre-wetting and unbending, and occurring at $T_{\mathrm{f}} < T < T_{\mathrm{w}}$, which is associated with the formation of a nanodroplet at the wedge apex. This is a so-called wedge pre-filling transition. In reality it is rounded by fluctuations, as is unbending. The mean-field pre-filling line of the wedge extends into the gas region of the wetting phase diagram, and runs tangentially to saturation, approaching it at T_{f} [52]. Interestingly, the remnant of wedge pre-filling is also picked up by DFT in the intermediate case of a 2D groove, formed by capping a slit pore [14]. More generally, geometrical patterning of the substrates enriches the wetting phase diagram. The additional transitions are highly sensitive to the interplay between the ranges of intermolecular forces and various fluctuation effects, such as thermally activated fluctuations and capillary waves. We point an interested reader to several recent in-depth investigations of wedge wetting that take into account these non-trivial effects [53, 54].

4. Conclusions

We have applied classical statistical mechanics in a mean-field DFT formulation to several prototypical cases of wetting on non-homogeneous substrates. As we have demonstrated, classical DFT offers a computationally accessible, rational and systematic means to incorporate fluid structure and the non-locality of the intermolecular fluid-substrate interactions into the robust mean-field thermodynamic method of van der Waals loops. Using DFT, one can easily obtain surface tensions and Young contact angles of macroscopic sessile drops adsorbed on flat homogeneous walls at bulk liquid-gas coexistence. Moreover, DFT allows one to probe fluid systems, all the way down to

the nanoscale, where the concept of Young angle becomes ill-posed. In particular, we have seen that flat substrates with narrow chemical stripes can adsorb nanodrops even below bulk saturation. Similarly, by considering wetting of a right-angle wedge, we have seen that the shape of the nanodrops adsorbed at the wedge apex is significantly affected by the substrate geometry. In general, due to the effects of non-local fluid-substrate intermolecular interactions, the menisci shapes and contact angles of nanodrops may significantly differ from the classical Young predictions.

Liquid adsorption is often associated with thermodynamic phase transitions occurring at the wall-gas interface. Our DFT computations illustrate how small-scale substrate inhomogeneities may affect the order of such transitions, a phenomenon that has ramifications at larger scales. For example, a chemical or structural impurity on a planar substrate can turn planar pre-wetting into a continuous transition. [But beyond the mean-field treatment, unbending transition could be rounded by the interfacial fluctuations and the formation of the nanodrops might be continuous].

The possible presence of metastable liquid (adsorbed on a chemical stripe or in a wedge apex) below bulk saturation may have important ramifications for heterogeneous nucleation. This is due to the fact that classical nucleation theories typically require bulk supersaturation for the condensation to occur. However, as we have seen, liquid may also be adsorbed on substrate impurities, due to the effects of small-scale non-local intermolecular interactions. Interestingly, the dynamics of phase transitions along such non-classical nucleation pathways may also be investigated in detail using the local-equilibrium modification of DFT. In particular, the recently developed fluctuating dynamical DFT, in principle, provides a theoretical framework capable of accounting for the effects of thermal fluctuations on the evolution of the system towards thermodynamic equilibrium [55].

Acknowledgments

We are grateful to Profs A.O. Parry and C. Rascón for numerous stimulating discussions. We acknowledge financial support from the Engineering and Physical Sciences Research Council (EPSRC) of the UK through Grants No. EP/L027186, EP/L020564, EP/L025159 and EP/K503733 (EPSRC-Imperial College Pathways to Impact-Impact Acceleration Award) and by the European Research Council (ERC) through Advanced Grant No. 247031.

References

[1] R. Seeman, M. Brinkman, E. J. Kramer, F. F. Lange, and R. Lipowsky. Wetting Morphologies at Microstructured Surfaces. *Proc. Natl. Acad. Sci. U. S. A.*, 102:1848, 2005.

[2] D. Bonn, J. Eggers, J. Indekeu, J. Meunier, and E. Rolley. Wetting and Spreading. *Rev. Mod. Phys.*, 81:739, 2009.

[3] K. Murata and H. Tanaka. Surface-Wetting Effects on the Liquid-Liquid Transition of a Single-Component Molecular Liquid. *Nat. Commun.*, 1:16, 2010.

[4] C. Rascón and A. O. Parry. Geometry-Dominated Fluid Adsorption on Sculpted Solid Substrates. *Nature*, 407:986, 2000.
[5] K. Binder. Modelling of Wetting in Restricted Geometries. *Annu. Rev. Mater. Res.*, 38:123, 2008.
[6] A. Checco, B. M. Ocko, M. Tasinkevych, and S. Dietrich. Stability of Thin Wetting Films on Chemically Nanostructured Surfaces. *Phys. Rev. Lett.*, 109:166101, 2012.
[7] A. O. Parry, C. Rascón, N. B. Wilding, and R. Evans. Condensation in a Capped Capillary is a Continuous Critical Phenomenon. *Phys. Rev. Lett.*, 98:226101, 2007.
[8] A. O. Parry, C. Rascón, E. A. G. Jamie, and D. G. A. L. Aarts. Capillary Emptying and Short-Range Wetting. *Phys. Rev. Lett.*, 108:246101, 2012.
[9] P. Yatsyshin, N. Savva, and S. Kalliadasis. Geometry-Induced Phase Transition in Fluids: Capillary Prewetting. *Phys. Rev. E*, 87:020402(R), 2013.
[10] C. Rascón, A. O. Parry, R. Nurnberg, A. Pozzato, M. Tormen, L. Bruschi, and G. Mistura. The Order of Condensation in Capillary Grooves. *J. Phys.: Condens. Matter*, 25:192101, 2013.
[11] P. Yatsyshin, N. Savva, and S. Kalliadasis. Wetting of Prototypical One- and Two-Dimensional Systems: Thermodynamics and Density Functional Theory. *J. Chem. Phys.*, 142:034708, 2015.
[12] A. O. Parry, C. Rascón, and A. J. Wood. Universality for 2D Wedge Wetting. *Phys. Rev. Lett.*, 83:5535, 1999.
[13] A. O. Parry, C. Rascón, and A. J. Wood. Critical effects at 3D wedge wetting. *Phys. Rev. Lett.*, 85:345, 2000.
[14] P. Yatsyshin, N. Savva, and S. Kalliadasis. Density Functional Study of Condensation in Capped Capillaries. *J. Phys.: Condens. Matter*, 27:275104, 2015.
[15] W. F. Saam. Wetting, Capillary Condensation and More. *J. Low Temp. Phys.*, 157:77, 2009.
[16] P. Yatsyshin, A. O. Parry, and S. Kalliadasis. Complete Prewetting. *J. Phys.: Condens. Matter*, 28:275001, 2016.
[17] M. Schick and P. Taborek. Anomalous Nucleation at First-Order Wetting Transitions. *Phys. Rev. B*, 46:7312, 1992.
[18] J. F. Lutsko and M. A. Durán-Olivencia. Classical Nucleation Theory from a Dynamical Approach to Nucleation. *J. Chem. Phys.*, 138:244908, 2013.
[19] J. F. Lutsko and M. A. Durán-Olivencia. A Two-parameter Extension of Classical Nucleation Theory. *J. Phys.: Condens. Matter*, 27:235101, 2015.
[20] M. A. Durán-Olivencia and J. F. Lutsko. Mesoscopic Nucleation Nheory for Confined Systems: A One-parameter Mode. *Phys. Rev. E*, 91:022402, 2015.
[21] D. Lohse and X. Zhang. Surface Nanobubbles and Nanodroplets. *Rev. Mod. Phys.*, 87:981, 2015.
[22] X. Zhang, Z. Lu, H. Tan, L. Bao, Y. He, C. Sun, and D. Lohse. Formation of Surface Nanodroplets Under Controlled Flow Conditions. *Proc. Natl. Acad. Sci. U. S. A.*, 112:9253, 2015.
[23] L. Bao, Z. Werbiuk, D. Lohse, and X. Zhang. Controlling the Growth Modes of Femtoliter Sessile Droplets Nucleating on Chemically Patterned Surfaces. *J. Phys. Chem. Lett.*, 7:1055, 2016.
[24] K. W. Schwarz and J. Tersoff. From Droplets to Nanowires: Dynamics of Vapor-Liquid-Solid Growth. *Phys. Rev. Lett.*, 102, 2009.
[25] R. E. Algra, M. A. Verheijen, L.-F. Feiner, G. G. W. Immink, W. J. P. van Enckevort, E. Vlieg, and E. P. A. M. Bakkers. The Role of Surface Energies and Chemical Potential during Nanowire Growth. *Nano Lett.*, 11:1259, 2011.
[26] T. M. Squires and S. Quake. Microfluidics: Fluid physics at the nanoliter scale. *Rev. Mod. Phys.*, 77:977, 2005.
[27] M. Rauscher and S. Dietrich. Wetting Phenomena in Nanofluidics. *Annu. Rev. Mater. Res.*, 38:143, 2008.
[28] Z. Gou and W. Liu. Biomimic From the Superhydrophobic Plant Leaves in Nature: Binary Structure and Unitary Structure. *Plant Sci.*, 172:1103, 2007.
[29] A. Calvo, B. Yameen, F. J. Williams, G. J. A. A. Soler-Illia, and O. Azzaroni. Mesoporous Films and Polymer Brushes Helping Each Other to Modulate Ionic Transport in Nanoconfined Environments. An Interesting Example of Synergism in Functional Hybrid Assemblies. *J. Am.*

Chem. Soc., 131:10866, 2009.

[30] D. Lohse and X. Zhang. Pinning and Gas Oversaturation Imply Stable Single Surface Nanobubbles. *Phys. Rev. E*, 91:031003, 2015.

[31] R. Evans. The Nature of the Liquid-Vapour Interface and Other Topics in the Statistical Mechanics of Non-Uniform, Classical Fluids. *Adv. Phys.*, 28:143, 1979.

[32] J. Wu. Density Functional Theory for Chemical Engineering: From Capillarity to Soft Materials. *AIChE J.*, 52:1169, 2006.

[33] J. F. Lutsko. Recent Developments in Classical Density Functional Theory. In *Adv. Chem. Phys.*, page 1. John Wiley & Sons, 2010.

[34] J. Landers, J. Yu. Gor, and A. V. Neimark. Density Functional Theory Methods for Characterization of Porous Materials. *Colloid Surface A*, 437:3, 2013.

[35] J. A. Barker and D. Henderson. Perturbation Theory and Equation of State for Fluids. II. A Successful Theory of Liquids. *J. Chem. Phys.*, 47:4714, 1967.

[36] D. E. Sullivan and M. M. Telo da Gama. Wetting Transitions and Multilayer Adsorption at Fluid Interfaces. In C. A. Croxton, editor, *Fluid Interfacial Phenomena*, page 45. Wiley, New York, 1986.

[37] P. Yatsyshin, N. Savva, and S. Kalliadasis. Spectral Methods for the Equations of Classical Density-Functional Theory: Relaxation Dynamics of Microscopic Films. *J. Chem. Phys.*, 136:124113, 2012.

[38] P. Yatsyshin and S. Kalliadasis. Mean-field Phenomenology of Wetting in Nanogrooves. *Mol. Phys.*, 114:2688, 2016.

[39] S. Dietrich. Wetting Phenomena. In C. Domb and J. L. Lebowitz, editors, *Phase Transitions and Critical Phenomena*, volume 12, page 2. Academic Press, 1988.

[40] D. Bonn and D. Ross. Wetting Transitions. *Rep. Prog. Phys.*, 64:1085, 2001.

[41] S. Dietrich. Structures in Fluids Induced by Interfaces. *J. Phys. Condens. Matter*, 8:9127, 1996.

[42] R. Evans. Density Functionals in the Theory of Nonuniform Fluids. In D. Henderson, editor, *Fundamentals of Inhomogeneous Fluids*, page 85. Marcel Dekker, New York, 1992.

[43] C. Ebner and W. F. Saam. New Phase-Transition Phenomena in Thin Argon Films. *Phys. Rev. Lett.*, 38:1486, 1977.

[44] R. Evans. *Fundamentals of Inhomogeneous Fluids*, chapter Density Functionals in the Theory of Nonuniform Fluids., page 85. Dekker, New York, 1992.

[45] C. Bauer, S. Dietrich, and A. O. Parry. Morphological Phase Transitions of Thin Fluid Films on Chemically Structured Substrates. *Europhys. Lett.*, 47:474, 1999.

[46] C. Rascón and A. O. Parry. Wetting on Non-planar and Heterogeneous Substrates. *J. Phys. Condens. Matter*, 12:A369, 2000.

[47] C. Bauer and E. Dietrich. Phase Diagram for Morphological Transitions of Wetting Films on Chemically Structured Substrates. *Phys. Rev. E*, 61:1664, 2000.

[48] C. Rascón and A. O. Parry. Surface Phase Diagrams for Wetting on Heterogenous Substrates. *J. Chem. Phys.*, 115:5258, 2001.

[49] P. Yatsyshin, A. O. Parry, C. Rascón, and S. Kalliadasis. Classical Density Functional Study of Wetting Transitions on Nanopatterned Surfaces. *J. Phys.: Condens. Matter*, 29:094001, 2017.

[50] E. H. Hauge. Macroscopic Theory of Wetting in a Wedge. *Phys. Rev. A*, 46:4994, 1992.

[51] K. Rejmer, S. Dietrich, and M. Napiorkowski. Filling Transition for a Wedge. *Phys. Rev. E*, 60:4027, 1999.

[52] A. Malijevský, and A. O. Parry. Density Functional Study of Compete, First-Order and Critical Wedge Filling Transitions. *J. Phys.: Condens. Matter*, 25:305005, 2013.

[53] A. Malijevský, and A. O. Parry. Critical Point Wedge Filling *Phys. Rev. Lett.*, 110:166101, 2013.

[54] A. Malijevský, and A. O. Parry. Filling Transitions in Acute and Open Wedges *Phys. Rev. E*, 91:052401, 2015.

[55] M. A. Durán-Olivencia, P. Yatsyshin, B. D. Goddard, and S. Kalliadasis. General Framework for Fluctuating Dynamic Density Functional Theory. *New J. Phys.*, 19:123022, 2017.